Icarus **143**, 425–428 (2000)
doi:10.1006/icar.1999.6312, available online at http://www.idealibrary.com on IDEAL®

NOTE

The Thermal Structure of Triton's Middle Atmosphere[1]

J. L. Elliot

Department of Earth, Atmospheric, and Planetary Sciences, and Department of Physics, Building 54-422, Massachusetts Institute of Technology, 77 Massachusetts Avenue, Cambridge, Massachusetts 02139-4307; and Lowell Observatory, 1400 West Mars Hill Road, Flagstaff, Arizona 86001-4499
E-mail: jle@mit.edu

D. F. Strobel

Department of Earth and Planetary Science, and Department of Physics and Astronomy, Johns Hopkins University, Baltimore, Maryland 21218

X. Zhu

Applied Physics Laboratory, Laurel, Maryland 20723; and Department of Earth and Planetary Science, Johns Hopkins University, Baltimore, Maryland 21218

and

J. A. Stansberry, L. H. Wasserman, and O. G. Franz

Lowell Observatory, 1400 West Mars Hill Road, Flagstaff, Arizona 86001-4499

Received June 8, 1999; revised October 29, 1999

The atmospheric structure of Triton in the altitude range 25–150 km shows an unexpectedly steep thermal gradient of 0.26 K km^{-1} above 50 km altitude, with a nearly isothermal profile below. The upper part of the profile can be explained by downward conduction of heat deposited by magnetospheric electrons and solar UV. However, the atmospheric temperature below 50 km is too cold for identified radiative processes to dispose of the inferred heat flux (0.0012 erg cm^{-2} s^{-1}) from the upper atmosphere. This implies that either the atmosphere is not in a steady state and/or an unidentified cooling mechanism is at work in the altitude range 25–50 km. When extrapolated to the surface, the inversion results yield a pressure of $19.0^{+1.8}_{-1.5}$ μbar, about 5μbar greater than that observed by Voyager.

Key Words: **Triton, atmospheres, occultations.**

From the *Voyager* Neptune–Triton flyby in 1989, measurements were made by the *Voyager* IRIS instrument that suggested a surface temperature of 38^{+3}_{-4} K (Conrath *et al.* 1989). The first report of the *Voyager* RSS results gave an equivalent isothermal temperature of the lower atmosphere of 48 ± 5 K and a surface pressure of 16 ± 3 μbar (Tyler *et al.* 1989), but later analysis revised these values to 42 ± 4 K and 14 ± 1 μbar (Gurrola 1995). *Voyager* UVS data implied that the upper atmosphere at ionospheric heights was isothermal at ∼100 K (Broadfoot *et al.* 1989). These three data sets were interpreted in terms of a radiative–thermal heat conduction model, where the principal atmospheric heating was solar EUV at ionospheric heights and the heat was conducted down to the surface where it was radiated away (Broadfoot *et al.* 1989). With further data analysis this model was refined to include heating by energetic magnetospheric electron precipitation (Strobel *et al.* 1990, Stevens *et al.* 1992), the addition of a troposphere below 10 km (Yelle *et al.* 1991, Stansberry *et al.* 1992), and CO rotational line cooling (Stevens *et al.* 1992, Krasnopolsky *et al.* 1993). These factors are used in the most comprehensive models based on *Voyager* measurements (Krasnopolsky and Cruikshank 1995, Strobel and Summers 1995, Strobel *et al.* 1996). More recently, Triton's atmosphere has been probed by stellar occulation observations (Olkin *et al.* 1997), and these have revealed an atmospheric expansion since the *Voyager* flyby, due to a temperature increase in the surface ice (Elliot *et al.* 1998).

In order to test the applicability of the radiative–conductive models to Triton's atmosphere, we have retrieved temperature profiles in the altitude range 25–120 km by applying numerical inversion techniques to the stellar occultation light curve (see Fig. 1) recorded with Fine Guidance Sensor (FGS) #3 aboard the Hubble Space Telescope in November 1997 (Elliot *et al.* 1998). The inversion equations used followed standard procedures (e.g., Wasserman and Veverka 1973), except that (i) we avoided the usual approximation that the atmospheric scale height is much smaller than the planetary radius, and (ii) we included horizontal focusing by the planetary limb.

The equations used are as follows:

$$\nu(r) = \exp\left[\frac{1}{\pi}\int_{\theta(r)}^{0} \cosh^{-1}(r'/r)\, d\theta(r')\right] - 1, \tag{1}$$

where $\nu(r)$ is the refractivity of the atmosphere as a function of radius r, r' is an integration variable, and θ is the angle that the starlight is refracted by Triton's atmosphere. We assume that the atmospheric composition does not vary with radius, so the number density $n(r)$ as a function of radius is given by

$$n(r) = \frac{N_0 \nu(r)}{\nu_{\mathrm{STP}}}, \tag{2}$$

[1] Based on observations with the NASA/ESA Hubble Space Telescope, obtained at the Space Telescope Science Institute, which is operated by the Association of Universities for Research in Astronomy, Inc. under NASA Contract NAS5-26555.

0019-1035/00 $35.00

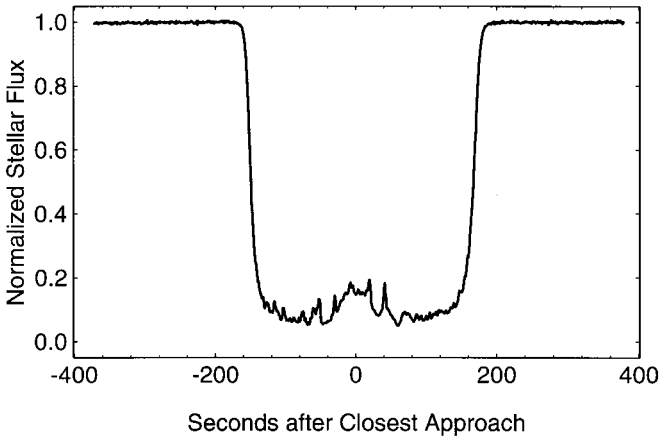

FIG. 1. Triton occultation of Tr180 as observed with FGS #3. The signals from all four PMT's were added together and the astrometric scan signature was removed to produce this occultation light curve, which is plotted relative to the time of closest approach of the HST to the center of Triton's occultation shadow. The photon noise in the data can be barely discerned on the pre- and post-occultation levels. The increase in signal near the center is due to the focusing of starlight by Triton's atmosphere near the center of the shadow. The irregular variations on the lower parts of the light curve are caused by small density fluctuations within the atmosphere, possibly due to turbulence created by convection.

where N_0 is Loschmidt's number and $\nu_{\rm STP}$ is the refractivity of N_2 (the major constituent of the atmosphere; Owen *et al.* 1993) under standard conditions. The inversion integral for the pressure as a function of radius, $p(r)$, is

$$p(r) = \frac{N_0 M_0 \mu G M_{\rm p}}{r\pi\,\nu_{\rm STP}} \int_{\theta(r)}^{0} \cosh^{-1}(r'/r) - \sqrt{1-(r/r')^2}\, d\theta(r'), \qquad (3)$$

where M_0 is the mass of one atomic unit, μ is the molecular weight of N_2, $M_{\rm p}$ is the mass of Triton, and G is the gravitational constant. The far-limb flux subtracted from the light curve prior to the inversion calculations was determined from a prior model fit to the entire light curve (Elliot *et al.* 1998). These fluxes agreed with those determined from the far-limb images in the astrometric scans. Other far-limb subtractions were tested, and the resulting temperature profiles proved to be insensitive to the choice, except for the lowest 5–10 kilometers. Radius steps used for the inversion ranged from a maximum of 4 km (determined by time resolution of the 1.0-s averaged data) to a minimum of 1 km at lower altitudes (Fig. 2). Error bars for the temperatures were calculated as described by French *et al.* (1978), but modified as appropriate for our small-planet inversion equations given above.

The immersion and emersion temperature profiles are shown in Fig. 2. Above a stellar flux of 0.5 (corresponding to an altitude of ~90 km) the profiles were established by fitting a model to the light curve that allows a thermal gradient (Elliot and Young 1992). These model fits were then used to determine the initial conditions for the inversions that established the profiles below 90 km. The effects of photon noise are indicated by the error bars, while imprecise knowledge of the minimum distance that the HST passed from the center of Triton's shadow introduces a systematic error in the altitude scale of a few kilometers, but has little effect on the temperatures. Although the photon noise has uncorrelated errors, the errors in the resulting temperatures are larger than the RMS scatter of the temperatures because the inversion procedure introduces a correlation. The analysis of the astrometric scans with FGS #3 after the occultation yields a closest approach distance of the HST to the center of Triton's shadow of 236 ± 51 km (without a center of body to center of light correction). The closest approach distance determined from the fit to the entire light curve for a circular figure yielded 224 ± 4 km (Elliot *et al.* 1998). Allowing an elliptical figure in the model fit gives 211 ± 3 km for the closest approach distance. The ellipticity of the atmospheric figure from this latter model fit is about 0.02, consistent with results from a previous occultation (Elliot *et al.* 1997). Details of that work will be presented later. For this analysis we use 224 ± 15 km for the closest approach distance to maintain numerical consistency with our previous analysis (Elliot *et al.* 1998), but the error bar is large enough to include the other determinations just discussed.

We attempted to adjust the parameters of a radiative–conductive model to fit the inversion profiles in Fig. 2, but without success. In this regard it is instructive to illustrate the basic properties of a radiative–thermal heat conduction model as a guide to understanding the implications of the stellar-occultation thermal profiles. In these modes CO and CH_4 are the radiatively active molecules, and information on the amounts of these in Triton's atmosphere has been established by *Voyager* (as discussed below). In Fig. 2 the most basic model incorporates ionospheric heating and chemical recombination heating above 145 km with the magnitude and profile discussed in Strobel and Summers (1995) and Strobel *et al.* (1996) with downward heat conduction. This model has approximately the correct magnitude for the temperature gradient above 50 km, but is much too warm in comparison with the measured thermal structure above 30 km. If we add the full heating and cooling associated with CH_4 (UV-photolysis heating, near-IR heating, and thermal-IR cooling in vibrational bands), then the temperature is elevated even further at all relevant altitudes. If instead, we add CO rotational

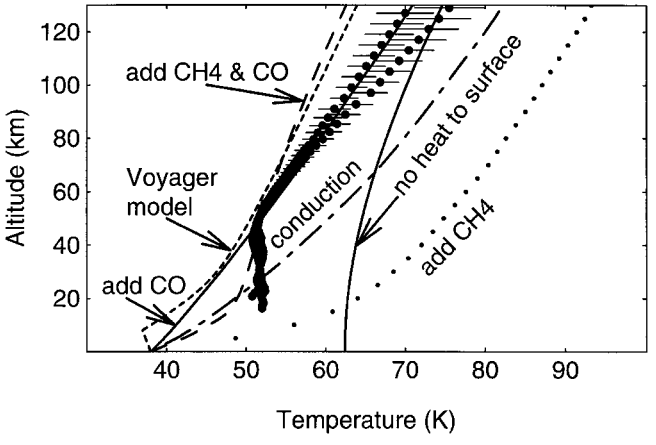

FIG. 2. Triton's thermal profiles compared with radiative–conductive models. Altitudes were calculated from radii for a surface radius of 1352 km. The larger points with error bars are a combined plot of (i) the temperatures (for altitudes above ~90 km) derived from the light curve model used to establish the initial conditions for the inversion calculations and (ii) the temperatures (below ~90 km) calculated from the inversions. The immersion profile is the cooler one at higher altitudes, but below ~80 km the profiles are virtually indistinguishable. The model profiles are as follows: (i) "conduction," (– – –) the most basic model, includes only ionospheric heating and chemical recombination heating above 145 km (Strobel and Summers 1995) and downward heat conduction to the surface; (ii) "add CO" (—, to left) adds to the "conduction" model CO rotational line cooling with a CO mixing ratio of 0.0002; (iii) "add CH4" (•••) adds to the "conduction" model recombination heating below 145 km, UV CH_4 photolysis heating, near-IR CH_4 heating, and thermal-IR cooling with a CH_4 profile based on *Voyager* UVS solar egress occultation (Herbert and Sandel 1991); (iv) "add CH4 and CO" (– – –) has CO mixing ratio of 0.002 and the "add CH4" CH_4 profile divided by a factor of 2; and (v) "no heat to surface" (—, to right) is the same as the "add CO" model, but with the constraint that no heat is conducted to the surface. Only the "add CO" model has the proper temperature profile above 50 km, but not below. The "add CH4 and CO" can match the nearly isothermal part of the inversion profiles but fails by a factor of 2 to match the derived temperature gradient above 50 km. The line labeled "Voyager model" (- - -) refers to a radiative–conductive model (Strobel *et al.* 1996) based on the *Voyager* results described at the beginning of the paper. The lowest 8 km in this model is a troposphere (Yelle *et al.* 1991), inferred primarily from observations of the plumes, which sets the lower boundary condition for the radiative–conductive calculations.

line cooling with a CO mixing ratio of 0.0002—which is only slightly higher than the mixing ratio of 0.00015 inferred from analysis of surface-ice spectra (Cruikshank *et al.* 1993)—then the calculated temperature profile is in agreement with the data above 50 km, but is too cold and not isothermal below 50 km. If we use the same amount of CO, but allow no heat flow to the surface (i.e., all heat conducted into the middle atmosphere from above must be radiated away), then the temperature required in the middle atmosphere is considerably higher than the observed values (Fig. 2). Combining both CO rotational line cooling with CO mixing ratio of 0.002 and full CH_4 heating and cooling with the *Voyager* UVS solar occultation egress CH_4 profile (Herbert and Sandel 1991) divided by a factor of 2, we obtain a nearly isothermal atmosphere ∼51 K from 25 to 50 km, but above 50 km a temperature gradient that is too small by a factor of 2. The latter effect results from the downward ionospheric heat flux being radiated away above 120 km by CO rotational line cooling. High CO mixing ratios produce isothermal conditions with CH_4 densities controlling the absolute value of temperature, whereas low CO mixing ratios permit temperature gradients above 50 km consistent with HST occultation data. We have considered and rejected additional radiatively active constituents such as HCN. Whereas its rotational line cooling would be extremely efficient, its vapor pressure at 50 K should be negligibly small. Thus we conclude that the class of radiative–thermal conduction models considered cannot explain the temperature profiles presented here.

An alternative explanation for the temperature profile below 50 km is that vertical mixing is driving the temperature gradient toward the adiabatic or saturated lapse rate (0.76 and 0.17 K km^{-1} for N_2, respectively), and that the region below 50 km is convective—a deep troposphere. Using a convective heating model (Stansberry *et al.* 1992, 1994), we find that tropospheric temperatures of 50 K can be achieved if there are now considerably more unfrosted regions in Triton's southern hemisphere than in 1989. To determine this, we examined a suite of models in which the *Voyager*-derived albedo (Stansberry *et al.* 1992) of a portion of Triton's surface was artificially darkened to represent the removal of a seasonal frost layer. We then computed the heating and cooling of the atmosphere by the surface, using the position of the Sun appropriate for 1997 (Stansberry 1998). Models in which a latitude band in the southern hemisphere was darkened were found to effectively heat the atmosphere. For example, a model in which the albedo was lowered to 0.2 in the latitude band 40° to 50°S gave an average atmospheric temperature at the top of the planetary boundary layer in excess of 50 K. Parameters describing the energy fluxes in that convection model are given in Table I, which reflect the assumption of no net atmospheric heating. The convective heat fluxes through the planetary boundary layer, which is less than 2 km thick, are roughly 10 times larger than in 1989 (Stansberry *et al.* 1992; see Table I). The stratospheric heat flux is about 4×10^{-4} of the downward convective heat flux and has no effect on the tropospheric thermal structure.

In order to achieve the 50-K temperature in the region 25–50 km required by the observations, one could make a small adjustment of parameters of the convection model (Table I) to achieve a small downward heat flow to the surface. Turbulent motions (eddies) above the boundary layer and below the tropopause in Triton's atmosphere would transport heat downward as a direct consequence of the isothermal (or any subadiabatic) temperature gradient. Indeed, the model requires the existence of such "free atmosphere" eddies to transport both the small stratospheric heat flux and the much larger upward convected heat flux back down to the surface in cold areas in order to conserve energy. However, such a closed circulation, with the heat sink located at the same pressure as the heat source, would violate Sandström's theorem (Defant 1961), which (applying the second law of thermodynamics) states that a closed steady-state circulation can be maintained in an atmosphere only if the heat source is at a higher pressure than the heat sink—otherwise viscous forces will eventually damp-out the circulation.

One way to satisfy Sandström's theorem would be to radiate away (within the troposphere) both the heat conducted downward from the ionosphere and the heat convected up from the surface. We investigated the effectiveness of CO and CH_4 (at the mixing ratios given earlier) for accomplishing this radiative cooling by computing a radiative–conductive model of the atmosphere under the assumption that the entire heat flux from the stratosphere had to be radiated away above the surface (the "no surface heat flow" model of Fig. 2). In contrast, the other radiative models in Fig. 2 each assumed that the stratospheric heat flux was removed at the tropopause by the convective mechanisms just discussed. Figure 2 shows that in order to radiate away just the stratospheric heat flux, the temperature of the lower atmosphere must be ∼63 K (much higher than the observed temperature of ∼50 K) and the temperature gradient above 50 km would be much too small. If we additionally require radiative cooling to account for even a small part of the upward convected heat flux, even higher temperatures would result. Thus the two radiatively active molecules, CH_4 and CO, explicitly included in our model appear to be insufficient to allow for a steady circulation driven by a combination of radiative cooling and convective heating. We have not identified any other likely constituents that would be abundant enough to provide the necessary cooling, nor have we investigated the effects of a nonuniform distribution of CO—although if CO were concentrated below 50 km, the qualitative effects on the radiative–conductive temperature profiles would be in the right direction. In the absence of a mechanism for producing a near-surface concentration of CO any such models would be entirely ad hoc.

TABLE I
Energy Fluxes

Quantity	Global average (erg cm^{-2} s^{-1})
Stratospheric heat flux (down)	0.0012
Convective heat flux (up)[a]	30
Convective heat flux (down)[b]	3.0
Insolation absorbed by frost[c]	81
Latent heat of sublimation[d]	0.7
Radiogenic heat flux from interior[e]	5.0 ± 1.6

[a] Over the dark areas with mean temperature of 57 K, which compose about 9% of the surface. If convection is not operating, the dark areas could be as cool as 50 K.

[b] Over the frost at 38 K, which composes about 91% of the surface.

[c] This is the part of the 1500 erg cm^{-2} s^{-1} arriving from the Sun at the distance of Triton that is calculated to be absorbed by the frost in order to balance all convective and radiogenic heat fluxes.

[d] The average amount of heat required to sublimate enough frost to increase the surface pressure from 14 to 19 μbar over 8.3 years.

[e] Brown *et al.* (1991).

Conceptually, one could envisage during the summer months on Triton the Sun sublimating the ice off the surface, lowering the surface albedo, raising the surface temperature, and initiating vigorous convection that increases the thickness of the troposphere. In the absence of any probable candidates for radiational cooling, eventually the tropopause heating shuts off convection and the troposphere increases in temperature until the atmosphere can radiate away the ionospheric heat flux. In the fall, the surface temperature decreases and the tropopause descends toward the surface. However, the time required for the downward conductive heat flux (0.0012 erg cm^{-2} s^{-1}) to heat the lower atmosphere from the observed value of 50 K to 63 K is nearly 800 years—much longer than other time constants for seasonal changes (Hansen and Paige 1992, Spencer and Moore 1992). So we could be observing an intermediate state in which the temperature gradient is slowly changing from the dry adiabat (caused by a spring convective surge) through isothermal, toward a conductive profile that will never be established.

Having determined the temperature profile in Triton's middle atmosphere, we have refined (Table II) our previous value for Triton's surface pressure in 1997. Our first analysis of these data (Elliot *et al.* 1998) established the surface pressure based on (i) the fit of a power law thermal-gradient model to the data to determine the pressure at a radius of 1400 km (48 km altitude), and (ii) extrapolation of this pressure to the surface using both a radiative–conductive model (Strobel *et al.* 1996) and a simple isothermal assumption. Our pressure at 1400 km radius based on the inversion is more accurate, but slightly lower than that from our global model fit (Elliot *et al.* 1998). We extrapolate the pressure at 1400 km (Table II) to the surface using the scale height at the lowest altitude probed by the inversion. Since the temperature must decrease to 38.0 K over the frost in some (but presently unknown) fashion, this method may slightly underestimate the surface pressure. The main contribution to the errors in the surface pressure

TABLE II
Triton's Atmospheric Structure

Quantity	Immersion	Emersion	Average
Geometry			
Sub-solar latitude (°)			−49.6
Sub-Earth latitude (°)			−49.4
Sub-occultation longitude (°)	10	206	
Sub-occultation latitude (°)	−5	−8	
Pressures			
Pressure at 1400 km (μbar)	$1.9^{+0.2}_{-0.1}$	$1.7^{+0.1}_{-0.2}$	$1.8^{+0.1}_{-0.1}$
Surface pressure (μbar)	$20.7^{+2.0}_{-1.8}$	$17.3^{+1.6}_{-1.3}$	$19.0^{+1.8}_{-1.5}$
Temperatures			
Gradient[a] (K km^{-1})	0.28	0.23	0.26
At 50 km (K)	51.5	51.6	51.6
Surface frost (K)			$38.0^{+0.2}_{-0.1}$
Surface dark area (K)			50–57

[a] Determined from the difference in inversion temperature at 50 and 90 km.

arise from the uncertainty in the closest approach distance as discussed above. Although one must extrapolate to calculate the surface pressure, the fact that the surface pressure has been increasing is firmly established through comparison of the half-light radii for two stellar occultations (Olkin *et al.* 1997, Elliot *et al.* 1998). A third stellar occulation, observed in July 1997, confirms this result (Sicardy *et al.* 1998). For a uniform surface-pressure increase of 5 μbar over the 8.3 years between the *Voyager* measurement and the occultation, the average latent heat required is about 0.23 of the downward convective heat flux (Table I). Consequently this latent heat has a significant role in the energy exchange between the atmosphere and surface. The predicted radiogenic heat from the interior (Brown *et al.* 1991) would also be significant (Table I).

Acknowledgments. We thank Ed Nelan for assistance with data reduction. The comments of referees Caitlin Griffith and Vladimir Krasnopolsky helped to clarify several issues. Peter Gierasch pointed out the relevance of Sandström's theorem, and Kerry Emanuel provided useful discussions about convection. D.F.S. thanks DESPA, Observatoire de Paris-Meudon for its hospitality during a portion of this research. Partial support for this work was provided by NASA, through grants NAG5-4859, NAG5-4168, and GO-07489 (the latter from the Space Telescope Science Institute, which is operated by AURA, Inc., under NASA Contract NAS5-26555).

REFERENCES

Broadfoot, A. L., S. K. Atreya, J. L. Bertaux, J. E. Blamont, A. J. Dessler, T. M. Donahue, W. T. Forrester, D. T. Hall, F. Herbert, J. B. Holberg, D. M. Hunten, V. A. Krasnopolsky, S. Linick, J. I. Lunine, J. C. McConnell, H. W. Moos, B. R. Sandel, N. M. Schneider, D. E. Shemansky, G. R. Smith, D. F. Strobel, and R. V. Yelle 1989. Ultraviolet spectrometer observations of Neptune and Triton. *Science* **246**, 1459–1466.

Brown, R. H., T. V. Johnson, J. D. Goguen, G. Schubert, and M. N. Ross 1991. Triton's global heat budget. *Science* **251**, 1465–1467.

Conrath, B., F. M. Flasar, R. Hanel, V. Kunde, W. Maguire, J. Pearl, J. Pirraglia, R. Samuelson, P. Gierasch, A. Weir, B. Bezard, D. Gautier, D. Cruikshank, L. Horn, R. Springer, and W. Shaffer 1989. Infrared observations of the Neptunian system. *Science* **246**, 1454–1459.

Cruikshank, D. P., T. L. Roush, T. C. Owen, T. R. Geballe, C. de Bergh, B. Schmitt, R. H. Brown, and M. J. Bartholomew 1993. Ices on the surface of Triton. *Science* **261**, 742–745.

Defant, A. 1961. The Sandström Theorem. In *Physical Oceanography*, pp. 489–492. Pergamon Press, New York.

Elliot, J. L., and L. A. Young 1992. Analysis of stellar occultation data for planetary atmospheres. I. Model fitting, with application to Pluto. *Astron. J.* **103**, 991–1015.

Elliot, J. L., H. B. Hammel, L. H. Wasserman, O. G. Franz, S. W. McDonald, M. J. Person, C. B. Olkin, E. W. Dunham, J. R. Spencer, J. A. Stansberry, M. W. Buie, J. M. Pasachoff, B. A. Babcock, and T. H. McConnochie 1998. Global warming on Triton. *Nature* **393**, 765–767.

Elliot, J. L., J. A. Stansberry, C. B. Olkin, M. A. Agner, and M. E. Davies 1997. Triton's distorted atmosphere. *Science* **278**, 436–439.

French, R. G., J. L. Elliot, and P. J. Gierasch 1978. Analysis of stellar occulation data. Effects of photon noise and initial conditions. *Icarus* **33**, 186–202.

Gurrola, E. M. 1995. *Interpretation of Radar Data from the Icy Galilean Satellites and Triton.* Ph.D. Thesis, Stanford University,

Hansen, C. J., and D. A. Paige 1992. A thermal model for the seasonal nitrogen cycle on Triton. *Icarus* **99**, 273–288.

Herbert, F., and B. R. Sandel 1991. CH_4 and haze in Triton's lower atmosphere. *J. Geophys. Res.* **96**, 19,241–19,252.

Krasnopolsky, V. A., and D. P. Cruikshank 1995. Photochemistry of Triton's atmosphere and ionosphere. *J. Geophys. Res.* **100**, 21,271–21,286.

Krasnopolsky, V. A., B. R. Sandel, F. Herbert, and R. J. Vervack 1993. Temperature, N_2, and N density profiles of Triton's atmosphere: Observations and model. *J. Geophys. Res.* **98**, 3065–3078.

Olkin, C. B., J. L. Elliot, H. B. Hammel, A. R. Cooray, S. W. McDonald, J. A. Foust, A. S. Bosh, M. W. Buie, R. L. Millis, L. H. Wasserman, E. W. Dunham, J. McDonald, L. A. Young, R. Howell, W. B. Hubbard, R. Hill, R. L. Marcialis, J. S. McDonald, D. M. Rank, J. C. Holbrook, and H. Reitsema 1997. The structure of Triton's atmosphere: Results from the entire ground-based occultation data set. *Icarus* **129**, 178–201.

Owen, T. C., T. L. Roush, D. P. Cruikshank, J. L. Elliot, L. A. Young, C. de Bergh, B. Schmitt, T. R. Geballe, R. H. Brown, and M. J. Bartholomew 1993. Surface ices and the atmospheric composition of Pluto. *Science* **261**, 745–748.

Sicardy, B., O. Mousis, W. Beisker, E. Hummel, W. B. Hubbard, R. Hill, H. J. Reitsema, P. Anderson, L. Ball, B. Downs, S. Hutcheon, M. Moy, G. Nielsen, I. Pink, and R. Walters 1998. Structure of Triton's atmosphere from the occulation of Tr176. *Bull. Am. Astron. Soc*. **30**, 1107.

Spencer, J. R., and J. M. Moore 1992. The influence of thermal inertia on temperatures and frost stability on Triton. *Icarus* **99**, 261–272.

Stansberry, J. A. 1998. Atmospheric control of Triton's frost distribution. *Bull. Am. Astron. Soc*. **30**, 1108.

Stansberry, J. A., J. I. Lunine, W. B. Hubbard, R. V. Yelle, and D. M. Hunten 1994. Mirages and the nature of Pluto's atmosphere. *Icarus* **111**, 503–513.

Stansberry, J. A., R. V. Yelle, J. I. Lunine, and A. S. McEwen 1992. Triton's surface–atmosphere energy balance. *Icarus* **99**, 242–260.

Stevens, M. H., D. F. Strobel, M. E. Summers, and R. V. Yelle 1992. On the thermal structure of Triton's thermosphere. *Geophys. Res. Lett*. **19**, 669–672.

Strobel, D. F., and M. E. Summers 1995. Triton's upper atmosphere and ionosphere. In *Neptune and Triton* (D. P. Cruikshank, Ed.), pp. 1107–1148. Univ. of Arizona Press, Tucson.

Strobel, D. F., A. F. Cheng, M. E. Summers, and D. J. Strickland 1990. Magnetospheric interaction with Triton's ionosphere. *Geophys. Res. Lett*. **17**, 1661–1664.

Strobel, D. F., X. Zhu, M. E. Summers, and M. H. Stevens 1996. On the vertical thermal structure of Pluto's atmosphere. *Icarus* **120**, 266–289.

Tyler, G. L., D. N. Sweetnam, J. D. Anderson, S. E. Borutzki, J. K. Campbell, V. R. Eshleman, D. L. Gresh, E. M. Gurrola, D. P. Hinson, N. Kawashima, E. R. Kursinski, G. S. Levy, G. F. Lindal, J. R. Lyons, E. A. Marouf, P. A. Rosen, R. A. Simpson, and G. E. Wood 1989. Voyager radio science observations of Neptune and Triton. *Science* **246**, 1466–1473.

Wasserman, L. H., and J. Veverka 1973. On the reduction of occultation light curves. *Icarus* **20**, 322–345.

Yelle, R. V., J. I. Lunine, and D. M. Hunten 1991. Energy balance and plume dynamics in Triton's lower atmosphere. *Icarus* **89**, 347–358.